AIMS Energy, 9(3): 534–557.
DOI: 10.3934/energy.2021026
Received: 16 January 2021
Accepted: 09 May 2021
Published: 17 May 2021

http://www.aimspress.com/journal/energy

Research article

Synergistic design of an integrated pv/distillation solar system based on nanofluid spectral splitting technique

Wei An*, Yifan Zhang, Bo Pang and Jun Wu

College of Mechanical Engineering, Tongji University, Shanghai, P.R. China

Correspondence: Email: anwei@tongji.edu.cn; Tel: +86-21-65983867.

Abstract: In the present work, an improved hybrid photovoltaic/distillation (PV/D) solar collector with nanofluid-based spectral splitting technique is redesigned by a synergistic design strategy to overcome the flaws of previous experiment system. In such a system, gold nanofluid plays a dual role as a heat absorption medium and a spectral splitting filter to enhance the distillation of water. This system can maximize the utilization of solar energy in whole spectrum, and can obtain electricity and freshwater simultaneously. However, the design of such an integrated hybrid system also become more complicated. Optical and thermal features of the system must be considered carefully and should be synergistically designed in the system. Specifically, an optical simulation is used to improve the configurations of the evaporator and increase the PV efficiency of the system. Another numerical model based on computational fluid dynamics is performed to optimize the layout of moist air circulation and enhance the condensation of vapor in the system. The experimental results confirmed the potential of nanofluid-based spectral splitting technique in solar distillation application. In comparison with the conventional system, the total efficiency of solar energy in the improved system with gold nanoparticles of 3.1 μg/mL, 10.2 μg/mL and 14.1 μg/mL concentration increases by 59.27%, 62.80% and 64.40%, respectively. The water yield per unit area of the improved system with different nanoparticle concentration increases by 35.32%, 37.59% and 42.62%, respectively. These results indicate that the improved system not only can realize the self-sufficiency, but also can carry out a flexible adjustment between PV and desalination units by changing the optical properties of the nanofluid. It can meet a versatile demand of power and heat in more extensive applications.

Keywords: Solar distillation; Spectral splitting; Nanofluid; PV/T

Nomenclature: A : area (m^2); B : atmospheric pressure (Pa); E : light homogeneity (%); G : direct solar irradiance (W/m^2); I : promotion rate of water yield (%); P : power (W); Q : energy (J); d : specific humidity (kg/kg(a)); m : water yield per unit area (ml/m^2); p : pressure (Pa); q : mass flow (kg/s); r : latent heat of vaporization (kJ/kg); t : time (s); η : efficiency (%); λ : wavelength (nm); ξ : empirical parameter in Eq (15); φ : relative humidity;

***Subscript*:** con: conventional solar distillation system; e: electronic; fan: fan; i: times; in: inlet; max: maximum; mean: mean value; net: net; nf: nanofluid; opt: optical; out: outlet; pv: pv cells; pvt: improved system based on pvt technique; s: saturated; th: thermal; tot: total; w: water;

***Superscript*:** ': actual value; p: produce; u: use

1. Introduction

Solar powered desalination techniques can use solar energy to convert the impure brackish water into potable drinking water. Due to the simple structure and low cost, solar distillation has drawn increasing concern as an effective way to solve the shortage of freshwater in some arid district [1–3]. However, it also suffers from some defects such as limited efficiency and low productivity [4–5]. From the perspective of the working mechanism of the basin desalination, intensification of evaporation and promotion of condensation can be considered to improve the performance of the conventional still.

Thermal characteristics of the working fluid significantly affect the performance of the distillation system. Compared to pure water, nanofluids consisting of nanometer-sized particles of metals, oxides, carbides, or graphite possess good thermal characteristics, which have led some researchers [6–14] to utilize different nanofluids in conventional solar distillation to enhance the evaporation process. Kabeel et al. [6] experimentally studied the effect of water nanofluids of Cu_2O and Al_2O_3 on the performance of solar still. The results obtained that using Cu_2O nanoparticles increased the distilled productivity by 93.87%, and using Al_2O_3 nanoparticles enhanced the distillate by 88.97%. Elango et al. [8] experimentally evaluated the performance of single basin single slope solar still with water and with water nanofluids of Al_2O_3, ZnO, Fe_2O_3 and SnO_2. The results showed that still with nanofluids has higher production, and still with Al_2O_3 nanofluid has 29.95% higher production. Due to the improved thermal transport and evaporation property by water nanofluid, as shown in Figure 1, solar distillation systems using nanofluids as the working fluids show significant improvements in productivity and thermal efficiency compared to the conventional distillation with pure water.

However, the enhancement of evaporation is only one of the critical process to promote the performance of solar distillation system, efficient production of freshwater also depends on the effective vapor condensation. The external condenser has been confirmed as an effective way to intensify the vapor condensation in solar distillation system [15]. Using separate PV panels to power the vacuum fan, Kabeel et al. [6] studied the effects of different nanofluids on the performance of solar still. The experimental results showed a considerably increase in the distillate water productivity. In fact, the external condenser not only can make full use of the released heat in vapor condensation process, but also improves the light transmittance of the distiller, so that more solar energy can be absorbed. However, the common external condensing process always requires an extra power to transport vapor and cooling water, which is difficult to implement in some areas lacking

electricity, such as small islands or remote mountain districts.

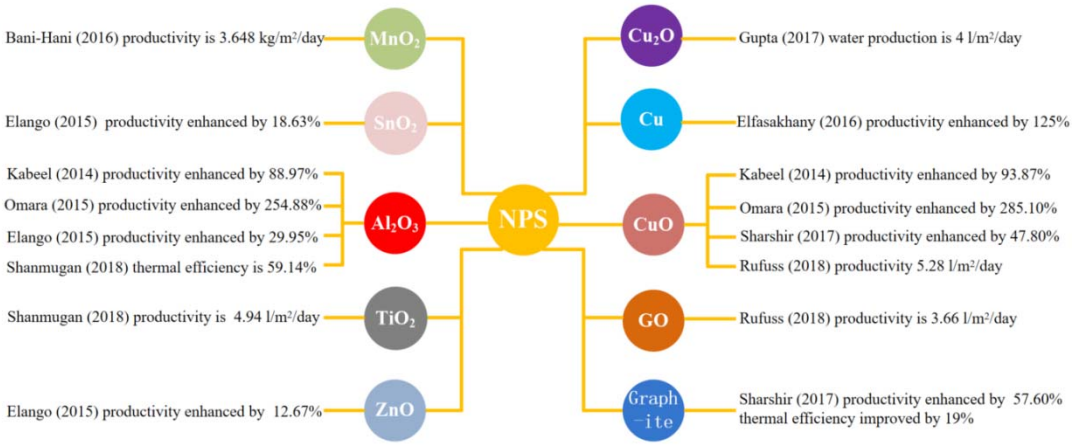

Figure 1. Application of nanofluids in solar distillation systems.

Recently, some scholars [16–21] proposed the hybrid solar systems that integrate photovoltaic (PV) module with distillation system to improve the performance of the conventional distillation system. These combined systems can not only provide energy for vapor transport, but also make use of the waste heat from PV module to increase the operating temperature of the salt water, and realize the simultaneous supply of freshwater and electricity with an efficiency that is higher than separate systems. In some districts with abundant solar energy resources but lack of fresh water, such as western of China, the integrated hybrid system has obvious advantages. Table 1 shows the recent advances and their performance of these integrated hybrid systems.

Researches on the hybrid PV/T solar distillation system are aimed to promote the performance of solar distillation and to realize an optimal integrated system with good respond for user requirements. As shown in Table 1, different thermal collectors were integrated with PV module in these researches, such as flat plate collector [16], active solar still [17] or evacuated collector [18]. These integrated system always can obtain a promotion of performance compared with a pure solar distillation system. Noting the spectral mismatch between PT and PV modules, An et al. [21] proposed an integrated hybrid PV/D solar collection system that combines a concentrating optical engineering and nanofluid-based spectral splitting (NSS) technique, where nanofluids with selectively spectral absorption are used as the working fluid to absorb solar radiation that can not be utilized by PV module and convert into heat to enhance evaporation. The experimental results showed that, compared with the conventional system, the water production of the system could increase by 79.9% and 69.4%, respectively, with only 26 μg/mL gold and silver nanofluids. However, due to ignoring the interaction between PV and distillation module, this preliminary experimental system also suffered from some obvious defects, such as very low photovoltaic efficiency and poor thermal efficiency. In this preliminary experiment, the power consumption of the condensation process exceeds the output of photovoltaic power generation. As a result, the system didn't achieve a complete self-sufficiency.

Table 1. Recent research on the hybrid photovoltaic/thermal (PV/T) solar distillation system.

Year	Authors	Experimental device	Daily water production
2010	Dev et al. [16]	Flat plate collector integrated with PV module.	7.22 kg/m^2/day
2010	Kumar et al. [17]	Hybrid PV/T active solar still.	7.22 kg/m^2/day
2016	Yari et al. [18]	Integrated translucent PV module and vacuum collector.	4.77 kg/m^2/day
2016	Al-Nimr et al. [19]	PV cells are placed at the bottom of the still basin and side fins serve as condensers.	6.8 kg/m^2/day
2018	Manokar [20]	PV cells are placed at the bottom of the still basin.	7.3 kg/m^2/day
2018	An et al. [21]	Combined a concentrating optical distiller and nanofluid-based spectral splitting PV/T technique.	Productivity enhanced by 79.9% than conventional still

In fact, the design of such a hybrid system becomes more complicated than a separated system. When integrating two sub-units of PV and distillation module into one system, the performance of both units and their interaction need to be considered, so that the two sub-units can perfectly cooperate with each other and work together to achieve the best performance of the hybrid system. Firstly, the spectral characteristics of nanofluid directly affects the allocation of solar energy in the PV and distillation units. Thus, the design of the hybrid PV/D system needs to carefully choose a suitable nanofluid whose spectral properties can be mediated easily to match the requirement of two sub-units. At the same time, some structural details of the solar collector also should be elaborately considered, especially the optical efficiency of collector and the light homogeneity on PV cells. In addition, a synergistic PV/D hybrid system not only needs to consider the optical performance of the solar collector, but also needs to consider the heat transfer between PV unit and distillation unit, so as to make full use of the waste heat generated by PV cells. Moreover, the heat and mass transfer in the hybrid system is also very important. High efficient heat exchange between vapor and cooling unit not only ensures the yield of pure water, but also directly effects solar energy transfer in the hybrid system, because the water-drop on the cover plate of distillation will decrease the transmittance of the cover plate. Therefore, the optical and thermal features of the system must be considered simultaneously in the design of the hybrid system. Significantly, the performance of the PV and distillation units also interact with each other. It is easy to observe from the fact that a higher water temperature is required to promote the evaporation process, but a higher temperature will reduce the efficiency of the PV unit. Thus, keeping a balance between two sub-units might be critical to achieve a successful design. What's more, the effects of different concentrations of nanofluids on the distillation and PV performance should be studied in depth to determine the appropriate conditions under which both stable power generation and high water production can be ensured. Unfortunately, these synergistic design concepts were not implemented in our previous work [21].

Therefore, the purpose of the present work is to promote the PV efficiency and water yield of the system by improving the evaporator configurations through synergistic design and to investigate the influence of nanoparticle concentration on the system performance. In order to improve the performance of the integrated PV/D system, the present study proposes a synergistic design flow, as shown in Figure 2, which consists of optical simulation, thermal transfer simulation and experimental verification. Firstly, an optical simulation is performed to improve the optical

performance of the evaporator. In addition, a numerical model based on computational fluid dynamics (CFD) is used to analyze the influence of moist air circulation channel on the vapor condensation. Both simulations are aimed at optimizing the solar collector configurations. Finally, the effects of different concentrations of gold nanofluids on the water yield and power generation performance of the improved system are investigated by a group of experiments.

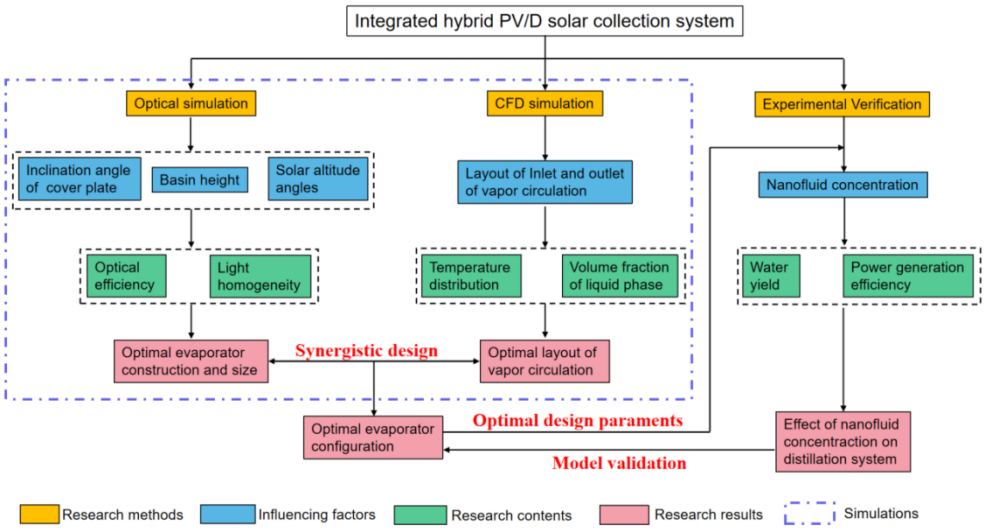

Figure 2. Schematic diagram of the research flow of the current study.

2. Design of experimental system

As shown in Figure 3, the improved integrated hybrid PV/D solar collection system based on NSS technique mainly consists of a basin-type evaporator, an external condenser, a PV cells unit, a centrifugal fan, a freshwater collection device, a battery unit, an inverter device and so on. When the NSS technique is applied in the PV/D solar distillation system, nanoparticles with selectively spectral absorption are added into water to absorb solar radiation that cannot be efficiently utilized by PV cells and convert it into heat to enhance evaporation. The rest of the solar radiation through the nanofluid is converted into electricity to drive the fan to promote the vapor condensation or to supply additional electricity to the power grid. At the same time, cooling water in the external condenser will absorb the heat released by the vapor and then be send into the basin-type evaporator.

In the following experiments, the glass cover of the evaporator is made of a piece of ultra-white glass with 0.15 m^2 area. The bottom of the sink is made of a transparent acrylic plate with an area of 0.13 m^2. The PV cells unit is composed of 24 pieces of monocrystalline silicon cells produced by Sun Power Corp., which are linked in series. They are tightly attached to the bottom of the sink and connected with a battery. The steam generated during the evaporation process is transported to the condenser by a centrifugal fan with 3.25 W power. In the condenser, several U-shape copper tubes with 20 mm inner diameter and 2.5 m total length are connected together and immersed into the water tank. The bottom of the U-shape copper tubes are connected with a collection device of condensed water. The outlet of the fan is connected with the condenser through a hose wrapped with 20 mm thick insulation, and then the outlet of the condenser is connected to the

other side of the distiller through another hose. In order to collect pure water as much as possible, a water channel is still set at the bottom of the glass cover to collect a small amount of water condensed on the cover plate.

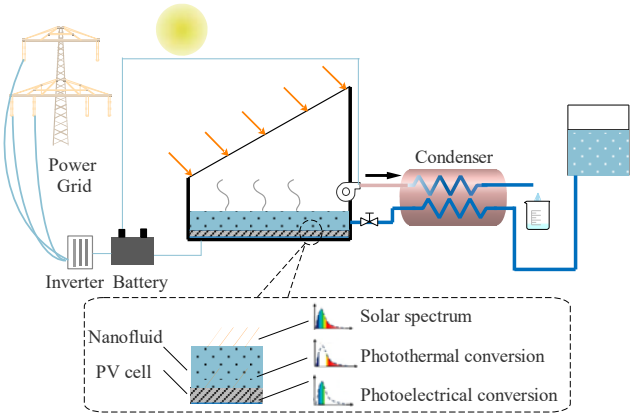

Figure 3. Schematic of the integrated hybrid PV/D solar collection system based on NSS technique.

2.1. Design of evaporator

In previous experiments [21], it can be found that the light concentrated structure increases the optical inhomogeneity on the PV cells, as shown in Figure 4b, though the light concentrated evaporator can realize a high water temperature. This flaw seriously affects the performance of the PV cells and leads to a low PV efficiency. As a result, the previous system failed to achieve self-sufficiency of electricity consumption.

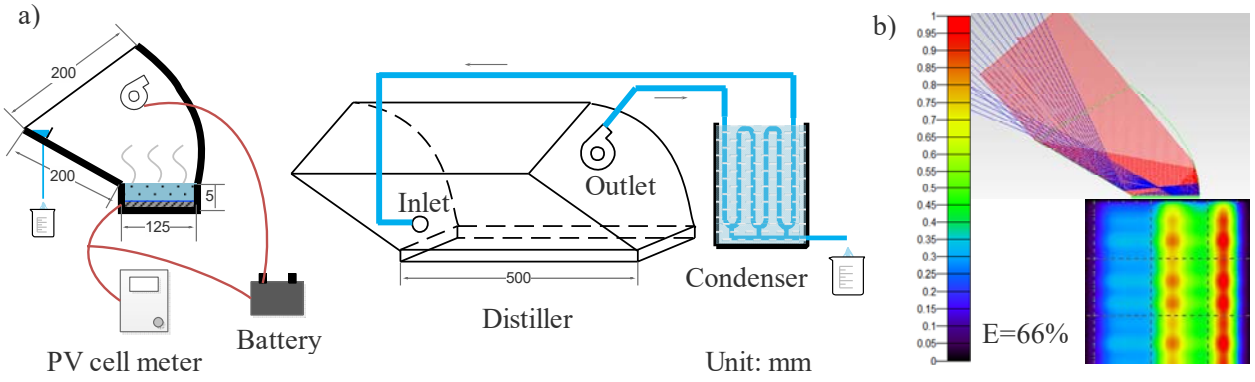

Figure 4. a) previous PV/D system with light concentrated design; b) optical simulation and the light homogeneity on the PV cells [21].

To overcome the flaw of the previous system, in the present work, we adopted an improved basin structure to replace the light concentrated design and used ray-tracing simulations based on Monte Carlo method to compare the optical performance of basin evaporators with different geometric structures. As shown in Figure 5, the improved evaporator is mainly composed of a glass cover plate, a front plate, a back plate, a transparent bottom plate and two side plates, and the PV

cells are arranged close to the bottom of the transparent bottom plate of the evaporation chamber. The inner surfaces of the back plate and the side plates are coated with a film with reflectivity of 0.80 to reflect the solar radiation to the bottom of the evaporator. In the ray-tracing simulation, the material properties of each part of the evaporator are shown in Table 2. In the model of distiller shown in Figure 5, the thickness of water is 10 mm, and the transmittance is set as 92.53%. The type of light source in the simulation is set as parallel beam, and the total number of rays is 1.5 million.

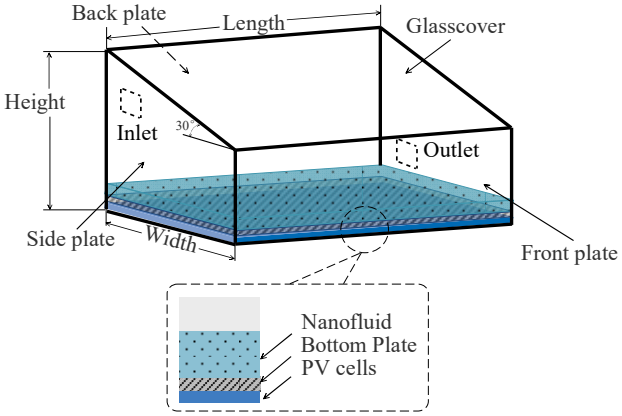

Figure 5. Schematic diagram of distiller structure.

Table 2. Geometric parameters and material properties of distiller.

Components	Geometric parameters	Optical properties
Cover plate	500 × 300 × 3 mm	Transmittance = 0.90, Refractive index = 1.46
Front plate	500 × 30 × 3 mm	Reflectivity = 0.80
Back plate	500 × 180 × 3 mm	Reflectivity = 0.80
Fluid	500 × 260 × 10 mm	Transmittance = 0.93, Refractive index = 1.33
Bottom plate	500 × 260 × 3 mm	Transmittance = 0.90, Refractive index = 1.46
PV cells	500 × 260 × 1 mm	Absorptivity = 1.00

In the optical simulations, two important parameters, namely the optical efficiency and the light homogeneity on the receiver surface, can be defined to characterize the optical performance of the basin evaporator. Firstly, the optical efficiency is the ratio of the incident energy flux to the received energy flux, so it is given as:

$$\eta_{\text{opt}} = q_{\text{w}} / q_{\text{in}} \tag{1}$$

where q_{in} and q_{w} are the energy flux on the surface of the glass cover and the bottom PV cells, respectively. Moreover, the light homogeneity on PV cells affects significantly on the performance of the cells. Thus, E defined in the following Eq (2), can be used to evaluate the homogeneity of the light spot on the receiver. The larger its value, the more uniform the light spot [21].

$$E = 1 - \frac{E_{\text{max}} - E_{\text{mean}}}{E_{\text{max}} + E_{\text{mean}}} \cdot 100\% \tag{2}$$

where E_{max} is the maximum radiant intensity on the receiver, and E_{mean} is the average radiant intensity.

It can be found from the results shown in Figure 6 that the optical efficiency and the light homogeneity on the surface of PV cells decrease gradually with the increase of the basin height. This indicates that the shading effect of the basin front plate on the sunlight becomes serious when the basin height increases. Compared with the basin with front plate height of 100 mm, the optical efficiency and the light homogeneity with front plate height of 20 mm increases by 4.19% and 7.40% respectively. At the same time, we also found that increasing the basin length could alleviate the shading effect of the side plate on the sunlight. Moreover, the optical efficiency of the evaporator has a declining tendency with the increase of the inclination angle of the cover plate. However, for the inclination angle of the cover plate, it should be considered that the collection of freshwater condensed on the cover plate in practical applications. Because the cover plate with a proper inclination angle can facilitate the freshwater condensed on it dropping into the collecting channel under the effect of gravity. Therefore, based on the above considerations, a basin with the cover plate of 30° inclination angle is adopted in the following experiments. In addition, the results in Figure 6 also shows that the light homogeneity of the improved evaporator is obviously better than that of the previous system, as shown in Figure 4b. This guarantees a promotion of PV cells performance in the following experiments.

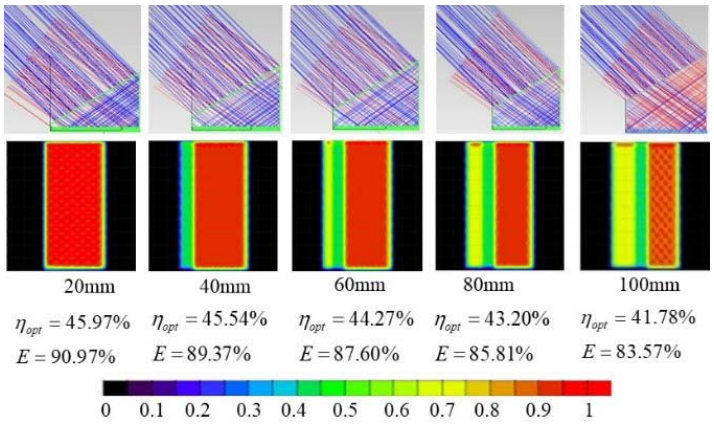

Figure 6. Optical model and light intensity contours on the PV cells with front plates of different height. The insert color map shows a normalized energy distribution on the bottom of the distiller.

2.2. Layout of moist air circulation

In a solar distiller system, an external condensing device can not only make full use of the heat released by vapor condensation, but also improve the light transmission of the cover plate, so that more solar energy can be collected in the evaporator. Therefore, depressing the vapor condensation on the cover plate will be beneficial to promote the system performance. It is always expected that most of the vapor in the evaporator can be transported to the external condenser. In the present experimental system, we installed a centrifugal fan in the evaporator to create a low-pressure zone on the outlet of moist air circulation and to transport the vapor to the external condenser. The non-condensable gas in the condenser will be returned to the evaporator through the inlet.

Accordingly, the layout of the inlet and outlet of the moist air circulation and the operation strategy of the fan become very important to the vapor condensation process, which directly affect the performance of the distillation system. Combined with the results of the above optical simulation, the inlet and outlet of the moist air circulation are arranged on the two side plates of the evaporator, respectively. However, the location of the two channels has an important impact on the temperature and flow of steam in the evaporator, which must be analyzed in detail. Therefore, a simplified computational fluid dynamics model was established by Fluent® software to analyze the effects of four different inlet and outlet arrangements on the evaporation performance, and thus determine the optimal inlet and outlet arrangements of the external condensation cycle.

The following simplifications and assumptions were made in the simulation. (1) In the numerical model, the inlet and outlet of the moist air circulation are simplified as squares with a side length of 50 mm. (2) The transparent cover plate on the top of the evaporator has no temperature gradient and is set as the Dirichlet boundary condition in the simulation. (3) The gas phase in the evaporator is set as ideal gas and the liquid phase as non-compressible fluid. (4) Except for the cover plate and the bottom plate, other plates of basin are set as adiabatic walls. The temperature and phase distribution in the evaporator cavity under steady state conditions with different inlet and outlet arrangements were analyzed using a multiphase flow based on the volume of fluid model [22]. The boundary conditions of this simulation are shown in Table 3.

Table 3. Boundary conditions in the numerical simulation.

Components	Boundary Type	Boundary Condition
Cover plate	Wall	Temperature = 308 K
Front plate	Wall	Heat flux = 0
Back plate	Wall	Heat flux = 0
Bottom plate	Wall	Temperature = 323 K
Inlet	Velocity-inlet	0.02 m/s, 300 K
Outlet	Pressure-outlet	−50 Pa，315 K
Side plate	Wall	Heat flux = 0

As shown in Figure 7, there are four available projects that can be adopted in practical applications. The inlet and outlet of the moist air circulation can be arranged at different locations near the back plate of basin. If the location features of the inlet and outlet are used as naming rule, these projects can be briefly named in four different cases: up-up, down-down, down-up and up-down, respectively.

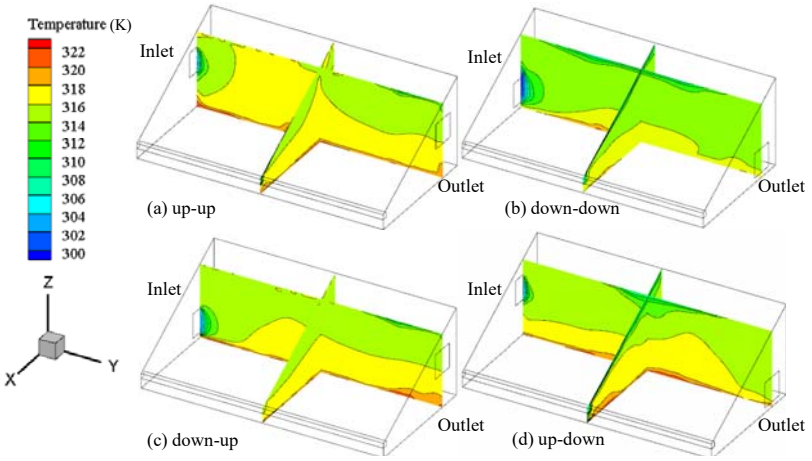

Figure 7. Temperature distribution on the different cross-sections of evaporator of four moist air circulation projects.

It can be found from the results shown in Figure 7 that the temperature distribution in the four cases shows a similar tendency: the temperature near the bottom of basin is higher, whereas the temperature on the inlet location has the lowest value. The up-up project has the highest average basin temperature, while this value becomes the lowest in the down-down project. Moreover, the volume fraction of liquid phase on the cover plate and the volume fraction of vapor phase on the outlet location are very important results, which can indicate the water and vapor distribution in the basin. An expected project should have a smaller value of the former and a larger value of the latter. Because this means that most of the vapor in the basin can be transported to the external condenser. From the results shown in Table 4, compared with the up-up and the down-down projects, the down-up and the up-down projects have a lower volume fraction of liquid phase on the cover plate. However, when the up-down project is considered, the volume fraction of vapor phase on the outlet location has a higher value than that of the down-up project. This means that the up-down project can achieve a high freshwater production in the external condenser. Notably, as can be seen from Figure 4a, the previous evaporator with light concentrated design used a layout that the water vapor outlet was on a higher location, and the inlet was on a lower location. According the above analysis, such a moist air circulation path is not the best option, because it may decrease the temperature level of the evaporator and thus inhibit the evaporation of water to some extent. Such a moist air circulation is also one of the reasons for the low water yield of the previous PV/D system. Therefore, in the following experimental system, the inlet of moist air circulation should be located near the glass cover of the basin, whereas the outlet of moist air circulation should be located near the bottom of the basin.

Table 4. Area-weighted average volume fraction on the different surfaces.

	up-up	down-down	down-up	up-down
Liquid phase on the cover plate (%)	4.3×10^{-3}	1.3×10^{-2}	1.1×10^{-4}	1.8×10^{-5}
Vapor phase on the outlet (%)	8.3×10^{-3}	1.3×10^{-3}	1.2×10^{-4}	3.3×10^{-3}

2.3. Control strategy of the circulating fan

As shown in Figure 8, a group of sensors and control units are installed in the experiment system to measure and adjust the moist air circulation. The control system consists of a microcontroller unit (Arduino Nano), a relay module, a K-type thermocouple module (MAX6675) and two temperature and humidity sensors (DTH22). The thermocouple is installed at the bottom of the sink, and the two DTH22 sensors are arranged at the inlet and outlet of the moist air circulation, respectively.

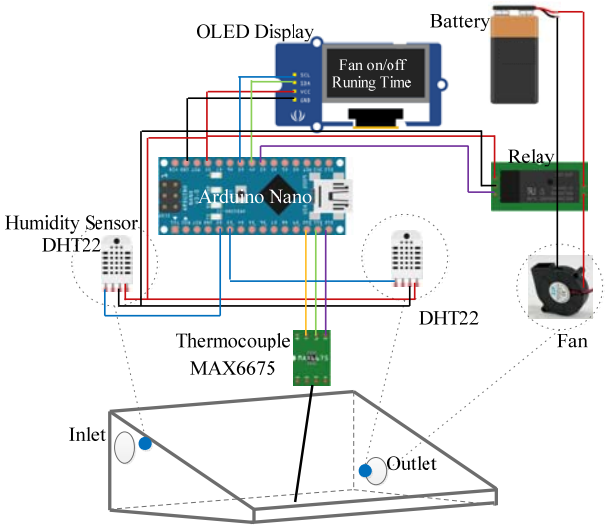

Figure 8. Schematic diagram of the vapor cycle control system.

In order to reduce the unnecessary energy consumption of the centrifugal fan, the fan can be turned on when the water temperature in the evaporator rises to 50 ℃ and turned off when the water temperature drops to 48 ℃ during the experiment. According to such a presupposed conditions, the fan is controlled by the relay and the microcontroller unit. The accumulated running time of the fan and the temperature and humidity of the vapor are recorded automatically by the microcontroller unit. Unfortunately, such a control strategy of the circulating fan was not implemented in our previous system [21], which led to excessive power consumption of the circulating fan. Therefore, the automotive control of circulating fan is also an effective approach to achieve self-sufficiency of the system.

2.4. Optical properties of nanofluids

In a spectral splitting hybrid system, the allocation of solar energy between the photothermal and photoelectric units is mainly decided by the optical window of spectral filter [23,24]. Therefore, the spectral characteristics of nanofluid play a vital role in the improved integrated hybrid PV/D solar distillation system based on the NSS technique. In the present system, the optical window of nanofluids can be seen as the waveband at which the fluid presents a high transmittance, while intensive absorption is expected at the waveband of except the optical window. According to the results of our previous study [24], gold and silver nanofluids are suitable for the improved distillation

application because of their good stability and adjustable spectral properties. In the present work, Au@SiO_2 core/shell nanoparticles were synthesized by the method of Lee et al. [25]. The statistics from TEM picture show that the gold particles with diameter of 24 to 38 nm occupy over 95%. These nanoparticles were diluted to form the nanofluids of different concentrations, which were employed in the following experiments. The optical transmittance of the gold nanofluid samples with different concentrations was measured by a UV-Visible-Near Infrared (UV-Vis-NIR) spectrometer. It can be found from the results shown in Figure 9 that gold nanofluids have a high transmittance at 700 nm to 1100 nm and a high absorption at 400 nm to 600 nm. Moreover, the absorptivity of these nanofluids at 400 to 600 nm rises with the increasing particle concentration. Comparatively, the transmittance of these nanofluids between 700 nm and 1100 nm keeps a slight change. Such spectral properties make them suitable to be employed in the improved integrated hybrid PV/D solar distillation system based on NSS technique.

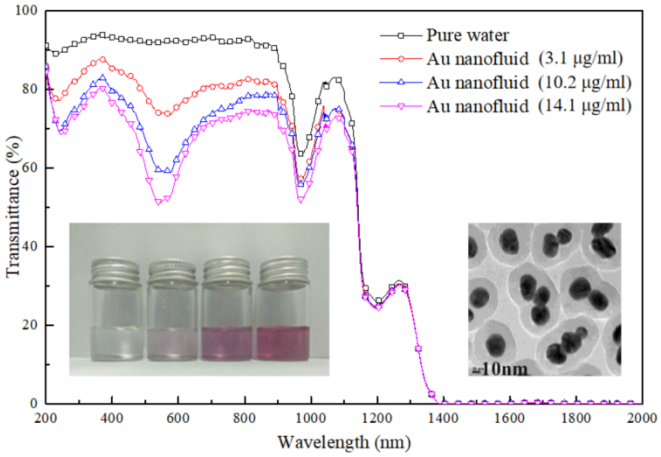

Figure 9. Spectral transmittance of pure water and gold nanofluids with different concentrations.

In order to evaluate the absorption effect of the nanofluids with different concentrations on solar energy, the mean absorptivity at 280 nm to 2000 nm waveband can be defined as Eq (3):

$$\bar{\alpha} = \int_{280}^{2000} G_{\mathrm{AM1.5}}(\lambda)\cdot[1-\tau(\lambda)]d\lambda \Big/ \int_{280}^{2000} G_{\mathrm{AM1.5}}(\lambda)d\lambda \tag{3}$$

where $G_{\mathrm{AM1.5}}$ presents the spectral intensity of solar radiation with 1.5 air mass, $\tau(\lambda)$ is the spectral transmittance of fluid. Similarly, the mean transmittance of fluids in the effective photovoltaic spectral waveband (280 nm to1200 nm) of crystalline silicon cells can be defined as the following Eq (4):

$$\bar{\tau}_{\mathrm{PV}} = \int_{280}^{1200} G_{\mathrm{AM1.5}}(\lambda)\cdot\tau(\lambda)d\lambda \Big/ \int_{280}^{1200} G_{\mathrm{AM1.5}}(\lambda)d\lambda \tag{4}$$

Compared with the results of pure water, the results shown in Table 5 indicate that the mean absorptivity of these nanofluids with different concentrations increase by 43% to 82%, while their

mean transmittance only decrease by 14% to 25% respectively. The effect of these optical properties on the performance of the improved distillation system will be discussed in the following section.

Table 5. Mean absorptivity and transmittance of fluids.

Property	Pure water	Au nanofluid (3.1 μg/mL)	Au nanofluid (10.2 μg/mL)	Au nanofluid (14.1 μg/mL)
Mean absorptivity	0.23	0.33	0.39	0.42
Mean transmittance	0.88	0.77	0.70	0.66

3. Experiment procedure and performance formulations

3.1. Experimental procedure

Four groups of experimental tests were performed to investigate the performance of the improved distiller system with different concentrations of gold nanofluids during 8:00–16:00 from April to July in 2019. Because of the different environmental conditions, a conventional basin distiller system with the same size was always used as a comparative reference in each test, as shown in Figure 10. The difference between the conventional distiller system and the improved system is that the conventional system does not have PV cells at the bottom, but its bottom is made of black opaque acrylic. In addition, the conventional system does not have an external condensation system for condensing water vapor. The experimental site is located on the roof of a building in college of mechanical engineering, Tongji University (31.23°N, 121.47°E). In the experiment, two K-type thermocouples were arranged in the sink of the two evaporators to measure the water temperature. Another two thermocouples were arranged on the glass cover of the two evaporators, and another thermocouple was used to measure the temperature of the PV cell in the improved system. A PV-cell meter is used to measure the characteristics of the PV cells. In the experiment, the temperatures of PV cell performance parameters and solar radiation were recorded every 10 minutes, and the water yield of the distillation system was recorded every 30 minutes by a measuring cylinder. The measuring instruments used in the experiment and their accuracy are shown in Table 6.

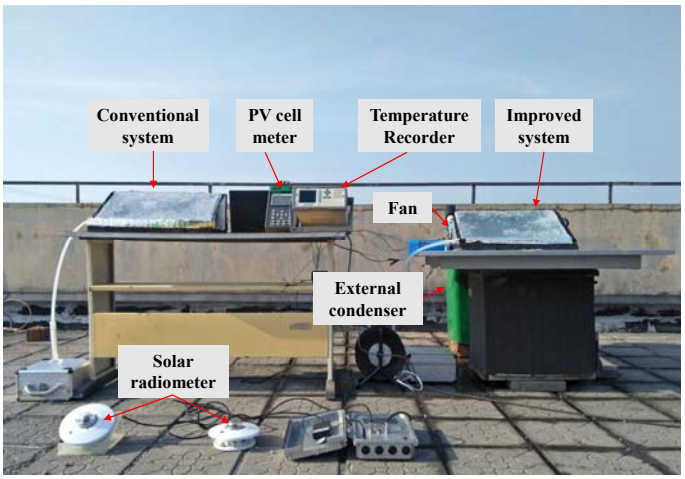

Figure 10. Picture of experimental system.

Table 6. Instruments and their accuracy.

Measured objective	Instrument	Accuracy
Transmittance of fluid	Shimadzu Ltd., Japan, UV3600	NA
Concentration of fluid	Agilent Technologies,USA,5100 ICP-OES	NA
Solar radiation	Jinzhou Sun technique Ltd., China, TBQ2B	<±2%
Solar cell meter	PROVA Instruments Inc., Taiwan, 210A	<±1%
Temperature	Applent Instruments Inc., China, AT4208	0.1 K
Humidity	Humidity Sensor DHT22	5%
Water yield	Measuring cylinder	0.1 mL

3.2. Mathematic formulations

There are four main parameters to evaluate the performance of the distillation system: water yield per unit area, thermal efficiency, electrical efficiency and total efficiency. Firstly, in order to compare the water yield per unit area of the conventional system and the improved system, the water yield per unit area of distillation system m is defined as Eq (5), where A_{w} is the area of the bottom of the evaporator, and m' is the measured water yield of the distillation system.

$$m = m'/A_{\mathrm{w}} \tag{5}$$

Then the promotion rate of water yield per unit area of the improved system compared with the conventional system I_{w} is expressed as:

$$I_{\mathrm{w}} = \left(m_{\mathrm{pvt}} - m_{\mathrm{con}}\right)/m_{\mathrm{con}} \tag{6}$$

where m_{con} and m_{pvt} represent the water yield per unit area of conventional system and the improved system, respectively. Secondly, the total solar radiation energy received by the distillation system is given by Eq (7):

$$Q_{\mathrm{inc}} = \sum_{i=1}^{n} G_i(t) \cdot A_{\mathrm{w}} \cdot \Delta t_i \tag{7}$$

where G_i represents the solar radiation measured for the i-th time, and Δt_i represents the time interval for measuring the solar radiation. The thermal energy effectively utilized in the conventional system can be expressed by Eq (8):

$$Q_{\mathrm{th}} = m' \cdot r \tag{8}$$

where r is the latent heat of vaporization of the fluid in the distiller. Whereas in the improved system, the heat released by the condensed steam need to be considered in the calculation of the thermal efficiency. Because this part of thermal energy is absorbed by water to be evaporated, it also belongs to the utilized thermal energy. Therefore, the thermal energy utilized in the improved system can be expressed by Eq (9):

$$Q_{\text{th}} = m' \cdot r + q_{\text{fan}} \cdot \left(h_{\text{in}} - h_{\text{out}}\right) \cdot \Delta t_{\text{fan}} \tag{9}$$

where Δt_{fan} is the running time of the fan during the test time; $h_{in} - h_{out}$ is the enthalpy difference between the inlet and outlet of the moist air circulation; q_{fan} is the mass flow of the fan. The enthalpy of the wet air at the inlet and outlet can be calculated by Eq (10):

$$h = 1.01 \cdot t + 0.001 \cdot d \cdot \left(2501 + 1.85 \cdot t\right) \tag{10}$$

where t is the temperature of the measuring point at the inlet and outlet of the moist air circulation; d is the specific humidity of the wet air, which can be calculated by Eq (11):

$$d = 0.622[\varphi p_{\text{s}} / (B - \varphi p_{\text{s}})] \tag{11}$$

where φ is the relative humidity at the measuring point. B is atmospheric pressure, p_{s} is the pressure of saturated steam at the measuring temperature. Then the thermal efficiency of the distillation system can be written as the ratio of Q_{th} and Q_{inc} :

$$\eta_{\text{th}} = Q_{\text{th}} / Q_{\text{inc}} \tag{12}$$

In the improved system, the electric energy generated by PV cells can be obtained by Eq (13):

$$Q_{\text{e}}^{\text{p}} = \sum_{i=1}^{n} P_i^{\text{pv}}\left(t\right) \cdot \Delta t_i \tag{13}$$

where P_i^{pv} is the power generation of the PV cell, and Δt_i is the time interval for measuring the performance parameters of the PV cell. The electric energy consumed by the fan can be given by Eq (14):

$$Q_{\text{e}}^{\text{u}} = \sum_{i=1}^{n} P_i^{\text{u}}\left(t\right) \cdot \Delta t_i \tag{14}$$

where P_i^{u} represents the power of the fan, and Δt_i is the operation time of the fan. Similarly, the net power generation efficiency of the improved system can be calculated as follows:

$$\eta_{\text{e}}^{\text{net}} = \left(Q_{\text{e}}^{\text{p}} - Q_{\text{e}}^{\text{u}}\right) \Big/ Q_{\text{inc}} \tag{15}$$

The conversion efficiency of PV cell of the improved system can be calculated by Eq (16):

$$\eta_{\text{e}}^{\text{pv}} = Q_{\text{e}}^{\text{p}} \Big/ \sum_{i=1}^{n} G_i\left(t\right) \cdot A_{\text{pv}} \cdot \Delta t_i \tag{16}$$

where A_{pv} is the area of the PV cell. Then, in order to evaluate the comprehensive performance of the system, the total efficiency of the hybrid system can be written as Eq (17):

$$\eta_{tot} = \frac{Q_{th} + \left(Q_e^p - Q_e^u\right)/\xi}{Q_{inc}} \tag{17}$$

where ξ is an empirical parameter and set as 0.38 [26]. This parameter is introduced based on the consideration that electricity is a higher grade of energy than thermal energy.

4. Results and discussion

4.1. Comparison of conventional and improved system

From 8:00–16:00 on April 5, 2019, we performed a comparative experiment with pure water between the improved system and the conventional system. Before the experiment, we put 1000 mL of pure water into both distillers. The curves of temperature and solar irradiance in the experiment are shown in Figure 11. At the beginning of the experiment, the water temperature and the glass cover temperature of both the conventional distiller and the enhanced distiller are increasing, and the tendency is similar for both systems. After the fan is firstly turned on at 10:05, the water temperature of the improved distiller keeps fluctuating between 48 ℃ to 50 ℃, while the temperature of the glass cover of the improved distiller is affected by the intermittent running of the fan, so the temperature fluctuation is more obvious than that of the water temperature. The maximum temperature of PV cell is 70.8 ℃ during the test. Although the solar radiation falls down rapidly after 14:00, the temperature of the PV cell still keeps slowly descending.

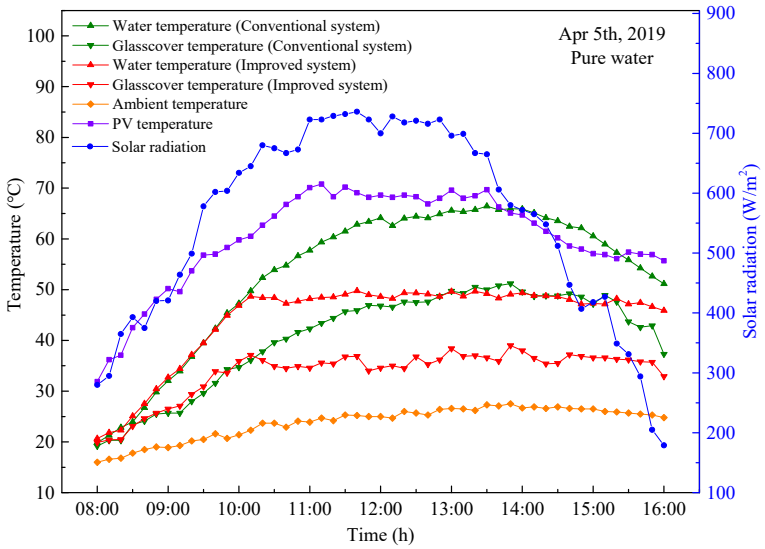

Figure 11. Temperatures in conventional and improved system with pure water.

The variation of water yield per unit area and fan operation time of the two system are shown in Figure 12. At the beginning of the experiment, the water yield per unit area of the improved system is approximately the same as that of the conventional system. With the increase of the solar radiation, the running time of the fan increases, the water yield of the improved system is higher than that of the conventional system gradually, and the promotion rate of water yield reached its maximum

at 12:00. During the experiment, the water yield per unit area is 1.91 L/m^2 and 2.42 L/m^2 for the conventional system and the improved system, respectively, and the water yield of the improved system was 26.61%, which is higher than that of the conventional system.

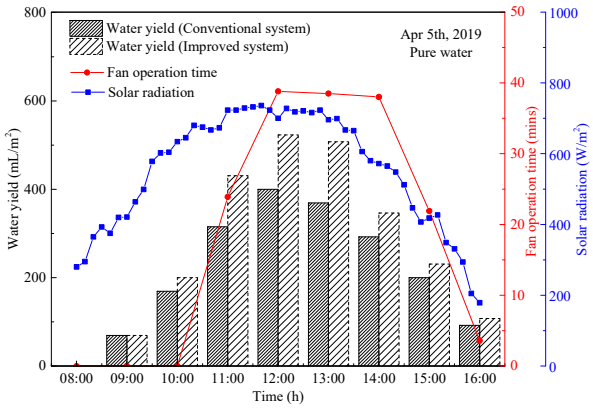

Figure 12. Water yield and fan operation time of conventional and improved system with pure water.

The variation of thermal efficiency, net power generation efficiency and total efficiency of the conventional and the improved systems are shown in Figure 13. It can be seen that the thermal efficiency of the improved system is significantly higher than that of the conventional system. The thermal efficiency of the conventional system reaches the maximum at 12:00, which is 35.10%; while the thermal efficiency and total efficiency of the improved system reaches the maximum at 13:00, which are 62.92% and 79.76%, respectively. At the same time, it can be seen that the power generation of PV cells in the improved system is far greater than the energy consumption of the fan, which can not only realize the self-sufficiency of the system, but also can provide power to the grid. The PV efficiency of the improved system reaches the maximum of 9.87% at 11:40. During the whole experimental process, the net power generation efficiency and total efficiency of the improved system are 5.43% and 56.85%, respectively.

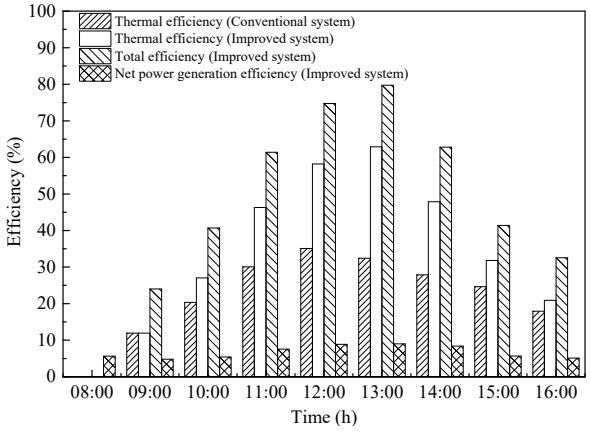

Figure 13. Thermal efficiency, net power generation efficiency and total efficiency of conventional and improved system with pure water.

4.2. Performance comparison of different nanofluid concentration

At 8:00–16:00 on May 3, May 5 and July 6, 2019, we carried out three groups of comparative experiments to investigate the effect of nanofluid concentration on the performance of the improved system. In three groups of experiments, gold nanofluid with the concentrations of 3.1 μg/mL, 10.2 μg/mL and 14.1 μg/mL were employed in the improved system and the conventional system, respectively. It can be found from Table 7 that the water yield, PV efficiency and thermal efficiency in the present improved system are much higher than those in our previous work. Compared with the previous work, the water yield is promoted by 27% to 79%, the PV efficiency is promoted by 519% to 414%, and the total efficiency is promoted by 111% to 130%, respectively for the results of 3.1 to 14.1 μg/mL concentration. Although the concentration of nanofluid is lower than that in the previous work, the performance of the present improved system shows a comprehensive superiority. Significantly, the present improved system achieves a net power generation even for the result of 14.1 μg/mL concentration.

Table 7. Performance comparison between the previous work and the improved system with different nanofluid concentrations.

Performance	Description	Au nanofluid [21]	Pure water	Concentration of Au nanofluids		
		26 μg/mL		3.1 μg/mL	10.2 μg/mL	14.1 μg/mL
m_{pvt} (l/m^2)	Water yield per unit area of the improved system	2.07	2.42	2.62	2.98	3.27
I_w (%)	Increase rate of water yield per unit area	79.9	26.61	35.32	37.59	42.62
η_e^{pv} (%)	Conversion efficiency of PV cell of the improved system	1.1	7.25	6.81	6.46	5.66
η_e^{net} (%)	Net power generation efficiency of the improved system	<0	5.43	4.46	3.51	2.88
η_{th}^{pvt} (%)	Thermal efficiency of the improved system	29.6	42.56	47.54	53.55	57.01
η_{th}^{pvt}-η_{th}^{con} (%)	Improved thermal efficiency compared with conventional system	6.8	15.74	19.74	25.64	29.02
η_{tot}^{pvt} (%)	Total efficiency of solar energy	28.1	56.85	59.27	62.80	64.60

Notably, the water yield per unit area of the improved system increases with the increase of the gold nanofluid concentration. This indicates that the addition of nanofluid can obviously promote the water yield of the system. On the other hand, the net generation efficiency of system decreases with the increase of the nanofluid concentration. However, the reduction of the net generation efficiency is only 2.55%, while the growth ratio of the water yield and the thermal efficiency are 35.12% and 14.45%,

respectively, when the nanofluid concentration increases from zero to 14.1 μg/mL.

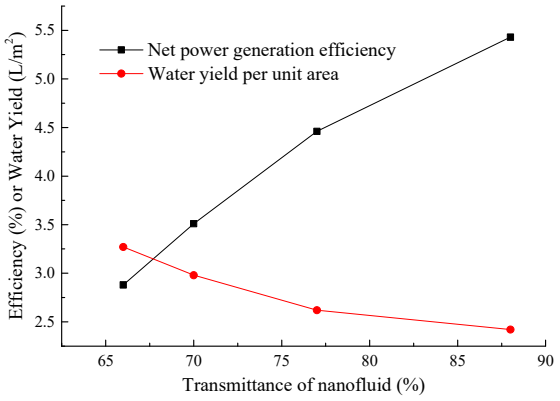

Figure 14. The variation of water yield and net power efficiency of the system with the transmittance of fluid.

Moreover, Figure 14 shows the variation trend of the water yield and net power generation efficiency with the mean transmittance of fluid. It can be seen from the results that the net power generation of the system gradually increases with the increase of the fluid transmittance, while a reverse trend can be found in the results of water yield. However, it is not a simple linear relationship between the two performances with the fluid transmittance. With the increase of the fluid transmittance, the variation rate of water yield and net power generation efficiency slow down gradually. This indicates that higher concentration of nanofluid has a greater impact on the performance adjustment of the hybrid system.

In addition, the variation of the water yield per unit area and the running time of the fan is shown in Figure 15. It can be seen that the total running time of the fan in the three groups of experiments is 219 minutes, 303 minutes and 209 minutes, respectively. This means that the running time of the fan might be mainly affected by the solar radiation and be independent of the nanofluid concentration. However, the water yield of the improved system was always higher than that of the conventional system. During the experimental process, the water yield of the improved system increased by 35.32%, 37.59% and 42.62%, respectively, compared to the conventional system. This indicates that the addition of nanoparticles has a significant effect on the improvement of water yield. Moreover, the transmittance of fluids decreases with the increase of the nanofluid concentration, so that the PV efficiency of system also declines gradually. During the whole experimental process, the PV efficiency of the improved system in the three experiments was 6.81%, 6.46% and 5.66%, respectively. Because of the increasing power consumption of the fan, the net generation efficiency in the three experiments decreased to 4.46%, 3.51% and 2.88%, respectively. However, the power generation of the PV cells in the improved system is always greater than the energy consumption of fans. Therefore, the improved system can always realize the self-sufficiency. The total efficiency of the improved system is 59.27%, 62.80% and 64.60%, respectively. These results confirm the potential of the integrated hybrid PV/D solar collector based on NSS technique, and the flexible adjustment performance of the improved distillation system as well.

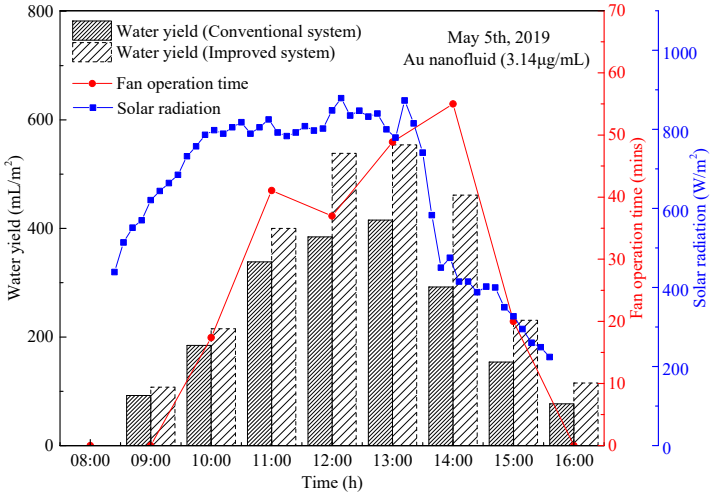

a) 3.1 μg/mL

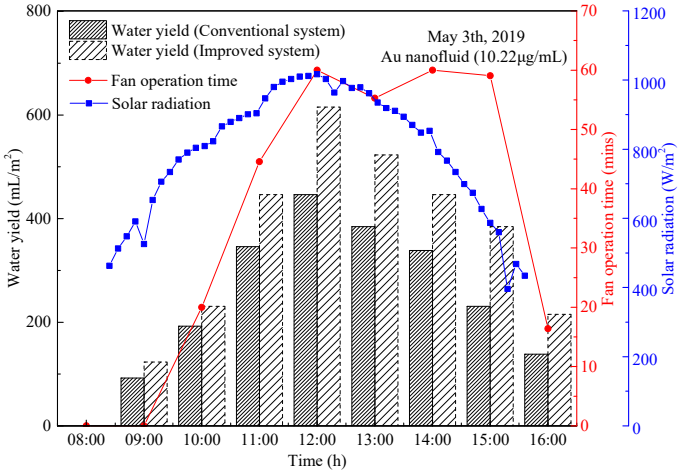

b) 10.2 μg/mL

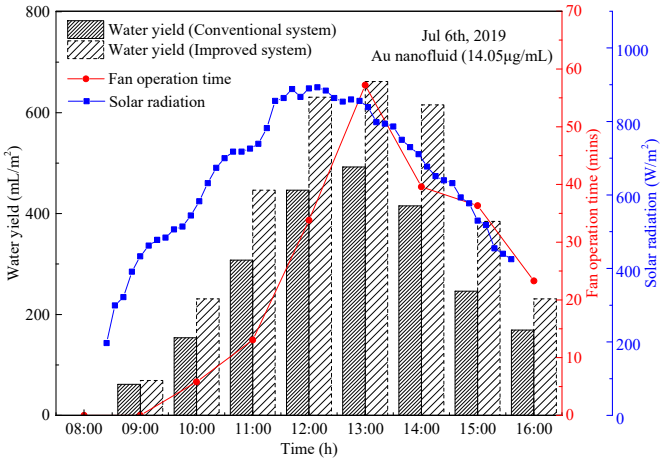

c) 14.1 μg/mL

Figure 15. Water yield and fan operation time of the improved system with different nanofluid concentrations.

4.3. Economic analysis

In order to evaluate the economics of the PV/D system, an economic study was conducted on the assumptions that the system can operate stably for 10 years and 300 days per year, and the cost of the land occupied by the system is not counting. If the average productivity of a conventional basin distillation system is 3.0–5.0 L/m^2/day [27], and that of our modified PV/D distillation system is about 5.0 L/m^2/day. Therefore, the total water production of the solar PV/D distillation system is 15000 L/m^2 during its life cycle.

The investment cost of the system is divided into construction cost and maintenance cost. As shown in Table 8, the total construction cost is about ¥1050/m^2. The cost of gold nanofluid with the concentration of 3.1 μg/mL, 10.2 μg/mL and 14.1 μg/mL required for the preparation of nanofluids is ¥4.08/L, ¥13.29/L and ¥18.27/L, respectively, which is the main maintenance costs. If the service life of these nanofluids is about 90 days, the total cost of the distillation system using different concentrations of gold nanofluid over 10 years is ¥1730/m^2, ¥3265/m^2 and ¥4095/m^2, respectively. Accordingly, the calculated cost of freshwater production is about ¥0.12/L, ¥0.22/L and ¥0.273/L for different nanofluid concentration, respectively.

Although the present calculation is still very rough, it still shows the economic potential of the integrated hybrid PV/D system. From the above calculations, it is clear that the cost of the PV/D system based on NSS technique depends mainly on the cost of the nanofluid and its lifetime. Although the cost of the present system is relatively high compared to other technologies, this does not mean that the present system loses its advantages. The relatively high freshwater production and the potential to provide both electricity and fresh water are still clear advantages of this system.

Table 8. Investment cost of each components constituting the integrated hybrid PV/D system.

System components	Cost (¥/m^2)
PV cells	400
Distillation module	100
External condenser	200
Lithium battery	150
Circulation pump and fan	100
Other devices	100

5. Conclusions

In the present work, an improved integrated hybrid PV/D solar distillation collector based on NSS technique was redesigned to overcome the flaws of previous experiment system by a synergistic method that involves both optical performance optimization and moist air circulation channel design. Specifically, an optical simulation for the evaporator was carried out to improve the PV efficiency. Another numerical model based on computational fluid dynamics was performed to redesign the layout of moist air circulation and promote the water yield.

The results indicate that the total efficiency of the improved system is approximately twice as high as that of the original one. Although the concentration of nanofluid is lower than that of the previous system, the performance of the present improved system shows a comprehensive superiority. These remarkable performance improvement can be ascribed to the modification of solar collector by

a synergistic design approach integrated the optical and thermal theories. In addition, the results also show that with the increase of the gold nanofluid concentration, the thermal efficiency and the water yield of the improved collector increase, but the power generation efficiency of PV cells decreases. However, there is not a simple linear relationship between the system performances with the fluid transmittance. Higher nanofluid concentration has a greater impact on the performance adjustment of the integrated hybrid collector.

The present experimental results not only confirm the application potential of solar PV/D distillation based on NSS technique, but also show that the improved distillation collector can realize a flexible adjustment between photovoltaic and desalination units by changing the optical properties of nanofluid. Although NSS-based PV/D technique has shown an attractive prospect, many technical problems in practical application are still very important. In particular, the design of integrated hybrid solar collector needs to combine optical and thermal analysis methods and consider the interaction of PV and distillation units. A synergistic design process that integrates the optical and thermal features of the system is vital to the performance promotion of the hybrid system.

Acknowledgements

This work was supported by the Natural Science Foundation of Shanghai (No. 20ZR1459600) and the Fundamental Research Funds for the Central Universities of China, all of which are gratefully acknowledged.

Conflict of interest

We declare that we have no any financial, personal or other relationships with other people or organizations that could inappropriately influence the manuscript entitled "Synergistic design of an integrated pv/distillation solar system based on nanofluid spectral splitting technique" by Wei An, Yifan Zhang, Bo Pang and Jun Wu.

References

1. Reif JH, Alhalabi W (2015) Solar-thermal powered desalination: Its significant challenges and potential. *Renewable Sustainable Energy Rev* 48: 152–165.
2. Sharon H, Reddy KS (2015) A review of solar energy driven desalination technologies. *Renewable Sustainable Energy Rev* 41: 1080–1118.
3. Kumar PV, Kumar A, Prakash O, et al. (2015) Solar stills system design: A review. *Renewable Sustainable Energy Rev* 51: 153–181.
4. He T, Yan L (2009) Application of alternative energy integration technology in sea water distillation. *Desalination* 249: 104–108.
5. Prakash P, Velmurugan V (2015) Parameters influencing the productivity of solar stills-A review. *Renewable Sustainable Energy Rev* 49: 585–609.
6. Kabeel AE, Omara ZM, Essa FA (2014) Enhancement of modified solar still integrated with external condenser using nanofluids: An experimental approach. *Energy Convers Manage* 78: 493–498.

7. Omara ZM, Kabeel AE, Younes MM (2014) Enhancing the stepped solar still performance using internal and external reflectors. *Energy Convers Manage* 78: 876–881.
8. Elango T, Kannan A, Murugavel KK (2015) Performance study on single basin single slope solar still with different water nanofluids. *Desalination* 360: 45–51.
9. Bani-Hani EH, Borgford C, Khanafer K (2016) Applications of porous materials and nanoparticles in improving solar desalination systems. *J Porous Media* 19: 993–999.
10. Elfasakhany A (2016) Performance assessment and productivity of a simple–type solar still integrated with nanocomposite energy storage system. *Appl Energy* 183: 399–407.
11. Rufuss DDW, Suganthi L, Iniyan S, et al. (2018) Effects of nanoparticle enhanced phase change material (NPCM) on solar still productivity. *J Clean Prod* 192: 9–29.
12. Shanmugan S, Palani S, Janarthanan B (2018) Productivity enhancement of solar still by PCM and nanoparticles miscellaneous basin absorbing materials. *Desalination* 433: 186–198.
13. Sharshir SW, Peng G, Wu L, et al. (2017) Enhancing the solar still performance using nanofluids and glass cover cooling: experimental study. *Appl Therm Eng* 113: 684–693.
14. Gupta B, Kumar A, Baredar PV (2017) Experimental investigation on modified solar still using nanoparticles and water sprinkler attachment. *Front Mater* 4: 23.
15. Kabeel AE, Omara ZM, Essa FA (2014) Improving the performance of solar still by using nanofluids and providing vacuum. *Energy Convers Manage* 86: 268–274.
16. Dev R, Tiwari GN (2010) Characteristic equation of a hybrid (PV-T) active solar still. *Desalination* 254: 126–137.
17. Kumar S, Tiwari A (2010) Design, fabrication and performance of a hybrid photovoltaic/thermal (PV/T) active solar still. *Energy Convers Manage* 51: 1219–1229.
18. Yari M, Mazareh AE, Mehr AS (2016) A novel cogeneration system for sustainable water and power production by integration of a solar still and PV module. *Desalination* 398: 1–11.
19. Al-Nimr MA, Al-Ammari WA (2016) A novel hybrid PV-distillation system. *Sol Energy* 135: 874–883.
20. Manokar AM, Winston DP, Kabeel AE, et al. (2018) Sustainable fresh water and power production by integrating PV panel in inclined solar still. *J Clean Prod* 172: 2711–2719.
21. An W, Chen L, Liu T, et al. (2018) Enhanced solar distillation by nanofluid-based spectral splitting PV/T technique: Preliminary experiment. *Sol Energy* 46: 146–156.
22. Rashidi S, Akar S, Bovand M, et al. (2018) Volume of fluid model to simulate the nanofluid flow and entropy generation in a single slope solar still. *Renewable Energy* 115: 400–410.
23. An,W, Li J, Ni J, et al. (2017) Analysis of a temperature dependent optical window for nanofluid-based spectral splitting in PV/T power generation applications. *Energy Convers Manage* 151: 23–31.
24. Ni J, Li J, An W, et al. (2018) Performance analysis of nanofluid-based spectral splitting PV/T system in combined heating and power application. *Appl Therm Eng* 129: 1160–1170.
25. Lee JE, Bera SP, Choi YS, et al. (2017) Size-dependent plasmonic effects of M and M@SiO_2 (M = Au or Ag) deposited on TiO_2 in photocatalytic oxidation reactions. *Appl Catal B- Environ* 214: 15–22.
26. Kumar BP, Winston DP, Poinraj P, et al. (2018) Experimental investigation on hybrid PV/T active solar still with effective heating and cover cooling method. *Desalination* 435: 140–151.

27. Prakash P, Velmurugan V (2015) Parameters influencing the productivity of solar stills—A review. *Renewable Sustainable Energy Rev* 49: 585–609.